Aisha Laguerre,[a]‡ Jerome Wielens,[a,b]‡ Michael W. Parker,[b,c]* Christopher J. H. Porter[d]* and Martin J. Scanlon[a]*

[a]Medicinal Chemistry and Drug Action, Monash Institute of Pharmaceutical Sciences, Monash University, 381 Royal Parade, Parkville, VIC 3052, Australia, [b]Structural Biology Laboratory, St Vincent's Institute, 9 Princes Street, Fitzroy, VIC 3065, Australia, [c]Department of Biochemistry and Molecular Biology, Bio21 Molecular Science and Biotechnology Institute, The University of Melbourne, 30 Flemington Road, Parkville, VIC 3010, Australia, and [d]Drug Delivery Disposition and Dynamics, Monash Institute of Pharmaceutical Sciences, Monash University, 381 Royal Parade, Parkville, VIC 3052, Australia

‡ These authors contributed equally to this work.

Correspondence e-mail: mparker@svi.edu.au, chris.porter@monash.edu, martin.scanlon@monash.edu
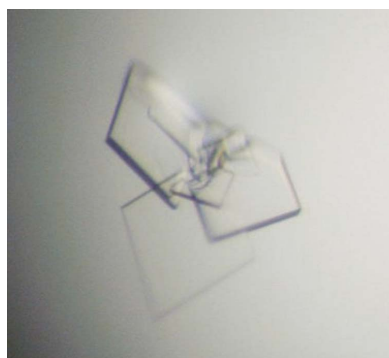
Preparation, crystallization and preliminary X-ray diffraction analysis of two intestinal fatty-acid binding proteins in the presence of 11-(dansylamino)undecanoic acid

Fatty-acid binding proteins (FABPs) are abundantly expressed proteins that bind a range of lipophilic molecules. They have been implicated in the import and intracellular distribution of their ligands and have been linked with metabolic and inflammatory responses in the cells in which they are expressed. Despite their high sequence identity, human intestinal FABP (hIFABP) and rat intestinal FABP (rIFABP) bind some ligands with different affinities. In order to address the structural basis of this differential binding, diffraction-quality crystals have been obtained of hIFABP and rIFABP in complex with the fluorescent fatty-acid analogue 11-(dansylamino)undecanoic acid.

1. Introduction

Fatty acid-binding proteins (FABPs) belong to the conserved multi-gene family of intracellular ligand-binding proteins (iLBPs; Furuhashi & Hotamisligil, 2008). Intestinal FABP (IFABP) is present at a high concentration in the absorptive cells of the intestine, where it is thought to participate in the uptake and transport of its hydrophobic ligands (Rowland *et al.*, 2009; Velkov *et al.*, 2005, 2007). All FABPs bind long-chain fatty acids, but differ in their ligand selectivity and binding affinity (Bernlohr *et al.*, 1997). An understanding of the factors that dictate the specificity of FABPs for binding to hydrophobic ligands will facilitate an improved understanding of intracellular transport pathways for endogenous hydrophobic ligands such as lipids, lipid-soluble vitamins and exogenous materials such as lipophilic drugs and xenobiotics. The members of the FABP family exhibit a highly conserved three-dimensional structure consisting of a β-barrel formed by ten antiparallel β-strands which is capped by two short α-helices. Various FABP structures, including those of hIFABP and rIFABP, have been solved by X-ray crystallography (Sacchettini *et al.*, 1989*a*,*b*; Young *et al.*, 1994; Marr *et al.*, 2006) and nuclear magnetic resonance spectroscopy (Zhang *et al.*, 2003; He *et al.*, 2007). These structures reveal that fatty acids bind within the β-barrel of the FABP binding pocket but that they do not occupy the full volume of the binding cavity. Despite overwhelming structural similarity, the identity of the amino-acid sequence between different human FABPs ranges from 15 to 67% (Chmurzynska, 2006).

IFABP contains a single ligand-binding site (Zimmerman & Veerkamp, 2002) which has a binding affinity (K_d) for long-chain fatty acids in the range 1–4 μM (Lowe *et al.*, 1987) and which also binds to a wider range of lipophilic compounds with similar or lower affinity (Rowland *et al.*, 2009; Velkov *et al.*, 2005, 2007). The amino-acid sequences of hIFABP and rIFABP are highly conserved (81% identity and 95% similarity), yet the two proteins have different affinities for some of their ligands (Rowland *et al.*, 2009; Velkov *et al.*, 2005, 2007). Although there are several available structures of hIFABP and rIFABP in both the apo state and in complex with long-chain fatty acids (LCFAs), the structural bases for these differences in affinity are not clear. There is evidence that even small changes in affinity may have important functional consequences. For example, a single-nucleotide polymorphism in hIFABP leads to the substitution of Ala54 with Thr (Baier *et al.*, 1995). This leads to an approximately twofold change in affinity for LCFAs, which appears to increase the

absorption and alter the processing of dietary fatty acids in the intestine and results in increased insulin resistance (Baier *et al.*, 1995, 1996). In an attempt to begin to address the structural basis of the observed differences in the affinity of hIFABP and rIFABP for some ligands, we have generated complexes of each protein bound to the same ligand. A comparison of these structures will assist in our understanding of the impact of residue differences between the rat and human variants on ligand-binding specificity. In this study, we report the crystallization of rIFABP and hIFABP in complex with the fluorescent fatty-acid analogue 11-(dansylamino)undecanoic acid (DAUDA).

2. Materials and methods

2.1. Cloning, expression and purification

The codon-optimized synthetic cDNA encoding hIFABP in the cloning vector pCR-Blunt was purchased from Retrogen (San Diego, California, USA). The hIFABP gene fragment was subcloned into a pET45b(+) expression vector (Invitrogen) using the *Kpn*I/*Bam*HI restriction-endonuclease sites. The cDNA for rat IFABP (rIFAPB) was excised from the pTrc99A expression vector (Velkov *et al.*, 2005) at the *Kpn*I/*Bam*HI restriction-endonuclease sites. The 408 bp rIFABP cDNA fragment was purified and ligated into *Kpn*I/*Bam*HI-digested pET45b(+) vector (Invitrogen). The cloning procedure introduced an N-terminal hexahistidine tag and three additional residues into each expression construct (generating MHHHH-HHVGT before the FABP sequence). The expression plasmids and their sequences have been deposited in the Addgene repository.

BL21 CodonPlus (DE3)-RIL Competent Cells (Stratagene, La Jolla, California, USA) were transformed with either rIFABP or hIFABP pET45b(+) plasmid and grown at 310 K in Luria–Bertani medium containing ampicillin (100 µg ml^{-1}) until an optical density at 600 nm of 0.6 was reached. Protein expression was induced in each case by adding isopropyl β-D-1-thiogalactopyranoside (1 mM) and the cultures were grown for a further 6 h and then harvested by centrifugation (14 000g for 15 min). The cell pellets were subjected to one freeze–thaw cycle (253 K for 12 h and thawing at room temperature) and were then lysed by sonication in buffer A (20 mM HEPES pH 7.0, 250 mM NaCl, 5 mM imidazole). Cell debris was removed by centrifugation (25 000g for 30 min) and the clarified supernatant was applied onto a HisTrap 5 ml column (GE Health-care, Sydney, Australia) at 5 ml min^{-1}. The column was washed with

buffer A and eluted with a gradient of 0–100% buffer B (20 mM HEPES pH 7.0, 250 mM NaCl, 0.5 M imidazole). The peak fractions were analysed by SDS–PAGE and those containing IFABP were pooled and ammonium sulfate was added to a final concentration of 2 M. The combined fractions were loaded onto a Phenyl Sepharose PHP 16/10 column (GE Healthcare, Sydney, Australia) in buffer C (20 mM MES pH 5.5, 50 mM NaCl, 2 M ammonium sulfate) and eluted with a gradient of 0–100% buffer D (20 mM MES pH 5.5, 50 mM NaCl).

rIFABP and hIFABP were delipidated by incubation with Lipo-philic Sephadex LH-20 100 (hydroxyalkoxypropyl beaded dextran; Sigma–Aldrich, Sydney, NSW, Australia) at 310 K for 3 h and then buffer-exchanged into buffer D on a HiPrep 26/10 desalting column (GE Healthcare, Sydney, Australia) and concentrated to 8 mg ml^{-1} using Amicon Ultra-4 5 kDa cutoff centrifugal filter devices (Milli-pore, Billerica, Massachusetts, USA). Protein concentrations were determined by UV spectrophotometry from measurement of the absorbance at 280 nm. The purity was assessed as >95% by SDS–PAGE analysis and the protein identity was confirmed by mass spectrometry, which revealed that the N-terminal methionine residue had been cleaved from the purified proteins but that the proteins were otherwise intact.

DAUDA was dissolved in dimethylsulfoxide to a concentration of 135.25 mM. This stock solution was then slowly added to the 8 mg ml^{-1} protein solution with frequent mixing to give an overall concentration of 8 mM DAUDA or an approximate 20-fold excess of ligand.

2.2. Crystallization and diffraction data measurement

Initial crystallization trials were carried out using sitting-drop vapour diffusion in 96-well plates (Greiner Low-Profile with two drops per well) and commercial screens including Crystal Screen, Crystal Screen 2, PEG/Ion, the Anions Screen and Grid Screen MPD from Hampton Research (San Diego, California, USA), Wizard I and II and Precipitant Synergy Screen from Emerald BioSciences (Bainbridge Island, Washington, USA), the PACT Suite and the JCSG+ Screen (Qiagen). The crystallization trials were set up using the Bio21 Collaborative Crystallization Centre (Bio21-C³, Parkville, Victoria, Australia). 100 nl protein solution (20 mM MES pH 5.5, 50 mM NaCl) and 100 nl precipitant solution were added together and equilibrated against 100 µl well solution at 281 K. Subsequent trials were carried out manually using hanging-drop vapour-diffusion
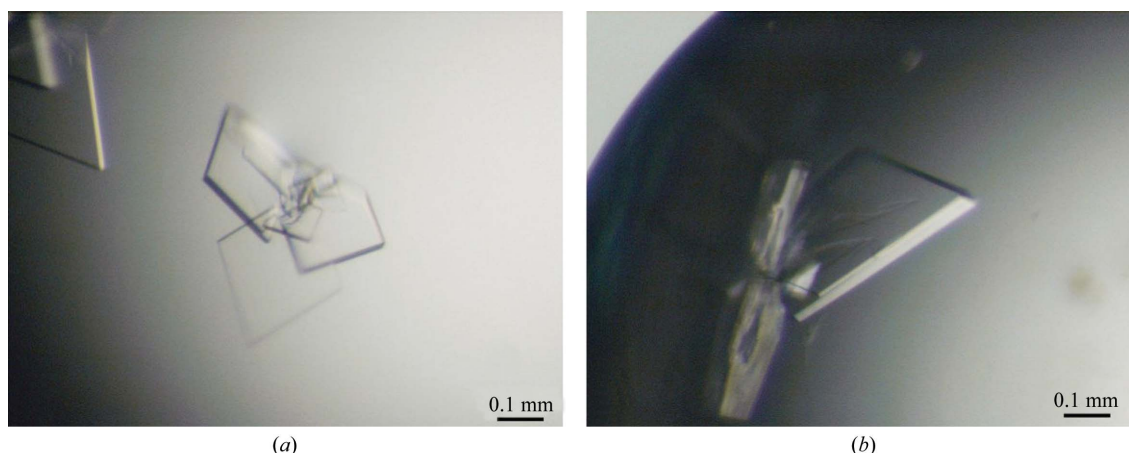

Figure 1
Crystals of FABP. (*a*) Crystals of hIFABP obtained in 32%(*w/v*) PEG 4000, 0.2 M MgCl$_2$ using the hanging-drop vapour-diffusion method. (*b*) Crystals of rIFABP obtained in 45% PEG 2000, 0.1 M Tris–HCl pH 7.0, 0.2 M MgCl$_2$ at 277 K.

Table 1
Summary of X-ray data measurement and processing statistics.

Values in parentheses are for the highest resolution shell.

	hIFABP	rIFABP
No. of crystals	1	1
Beamline	MX1	MX1
Wavelength (Å)	0.954	0.954
Temperature (K)	100	100
Crystal-to-detector distance (mm)	170	150
Exposure time (s)	3	2
No. of images	360	720
Oscillation range (°)	0.5	0.5
Space group	$P2_1$	$P4_32_12$
Unit-cell parameters (Å, °)	$a = 51.0$, $b = 79.0$, $c = 63.2$, $\beta = 94.5$	$a = b = 50.6$, $c = 97.5$
Solvent content (%)	41.2	41.9
Resolution range (Å)	50.8–1.9 (2.0–1.9)	44.9–1.6 (1.7–1.6)
Mosaicity (°)	0.8	0.2
No. of observations	143933 (20911)	484826 (70176)
No. of unique reflections	39319 (5728)	17480 (2499)
Completeness (%)	99.5 (99.7)	100 (100)
Multiplicity	3.7	27.7
R_{merge}† (%)	9.9 (48.6)	5.6 (38.2)
Mean $I/\sigma(I)$	8.8 (2.4)	42.0 (10.1)
Wilson B factor (Å^2)	19.1	20.4

† $R_{merge} = \sum_{hkl} \sum_i |I_i(hkl) - \langle I(hkl) \rangle| / \sum_{hkl} \sum_i |I_i|(hkl)$.

methods (McPherson, 1982). Drops consisting of 2 µl protein solution at a protein concentration of 8 mg ml^{-1} and 2 µl precipitant were equilibrated against 1 ml well solution at 277 K using 24-well Linbro plates and 22 mm siliconized cover slips (Hampton Research, San Diego, California, USA).

2.3. X-ray diffraction

Diffraction data were collected at 100 K on the MX1 beamline at the Australian Synchrotron. Reflections were measured using an ADSC Quantum 210r detector and the *Blu-Ice* interface (McPhillips

et al., 2002). For both complexes, the conditions in the hanging drop provided sufficient cryoprotection. The data were indexed using *MOSFLM* (Leslie, 1992) and scaling was performed using *SCALA* (Evans, 2006) in the *CCP*4 interface (Collaborative Computational Project, Number 4, 1994).

3. Results and discussion

3.1. Human IFABP

In the initial 96-well format crystallization screen, small clusters of crystals were observed in a number of conditions containing various molecular-weight polyethylene glycol (PEG) solutions at 281 K. Very thin plates were found in a well containing 0.2 *M* NaCl, 0.1 *M* HEPES pH 7.5, 30%(*w/v*) PEG 400; however, they failed to diffract beyond 8 Å resolution. Thicker plates of dimensions 0.4 × 0.3 × 0.02 mm were obtained using hanging drops with 32%(*w/v*) PEG 4000, 0.2 *M* MgCl$_2$ at 277 K. Crystals appeared after 2 d and reached their final dimensions within 3–4 d (Fig. 1*a*). Crystal growth and stability were temperature-sensitive and no diffraction beyond 8 Å resolution was obtained for crystals grown at room temperature for either protein–DAUDA complex. X-ray diffraction data from a single crystal were collected to 1.8 Å resolution on the MX1 beamline at the Australian synchrotron (Fig. 2). The crystal-to-detector distance was 170 mm. Data-collection statistics are shown in Table 1. The crystal belonged to space group $P2_1$, with unit-cell parameters $a = 51.0$, $b = 79.0$, $c = 63.2$ Å, $\beta = 94.5°$. The calculated Matthews coefficient (Matthews, 1968) predicted either three or four molecules in the asymmetric unit. [For three molecules $V_M = 2.79$ Å^3 Da^{-1}, corresponding to a solvent content of 55.9%, with a probability $P_{(tot)}$ of 0.42. For four molecules $V_M = 2.09$ Å^3 Da^{-1}, corresponding to a solvent content of 41.2% with a probability $P_{(tot)}$ of 0.55. A molecular mass of 15 188 Da was used.] The hIFABP structure was solved by molecular replacement using *Phaser* (McCoy *et al.*, 2007) with the hIFABP NMR structure (PDB
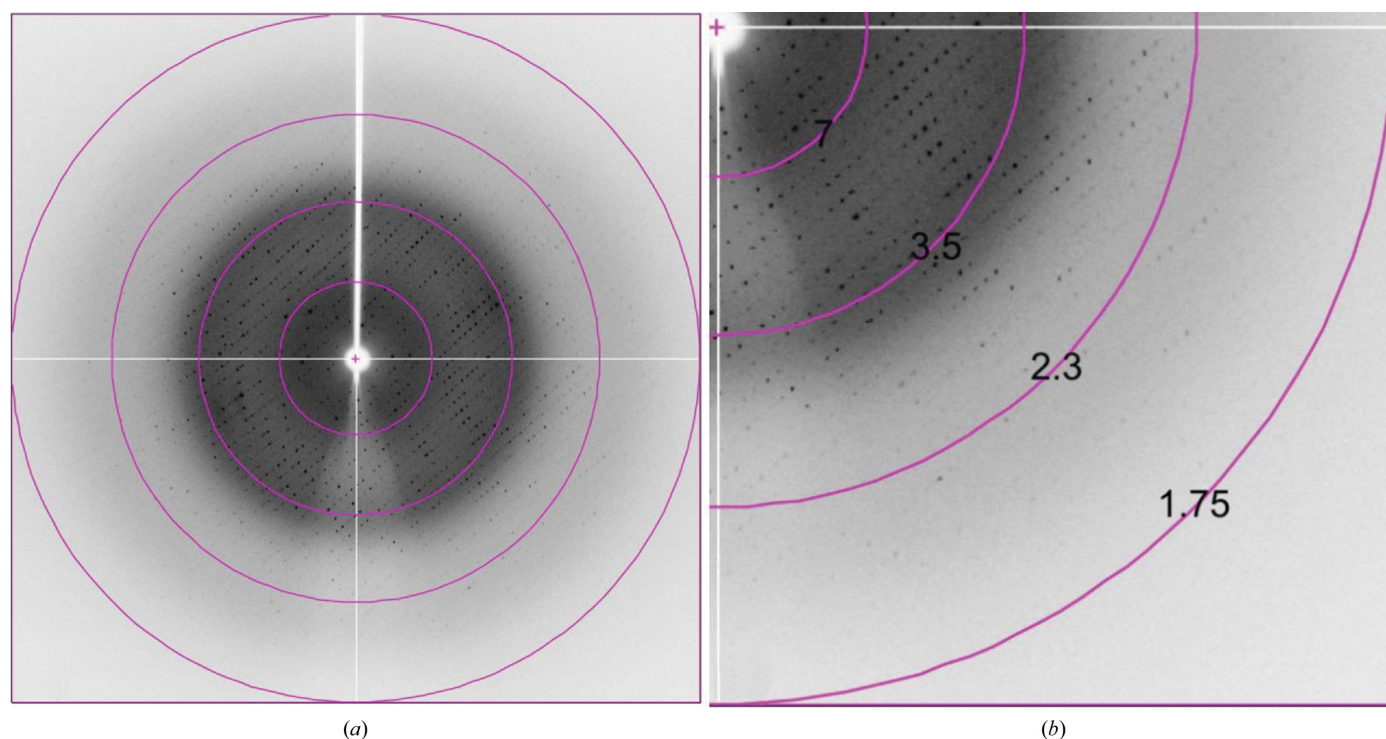

(*a*)   (*b*)

Figure 2
Diffraction image of an hIFABP crystal obtained at the Australian Synchrotron.
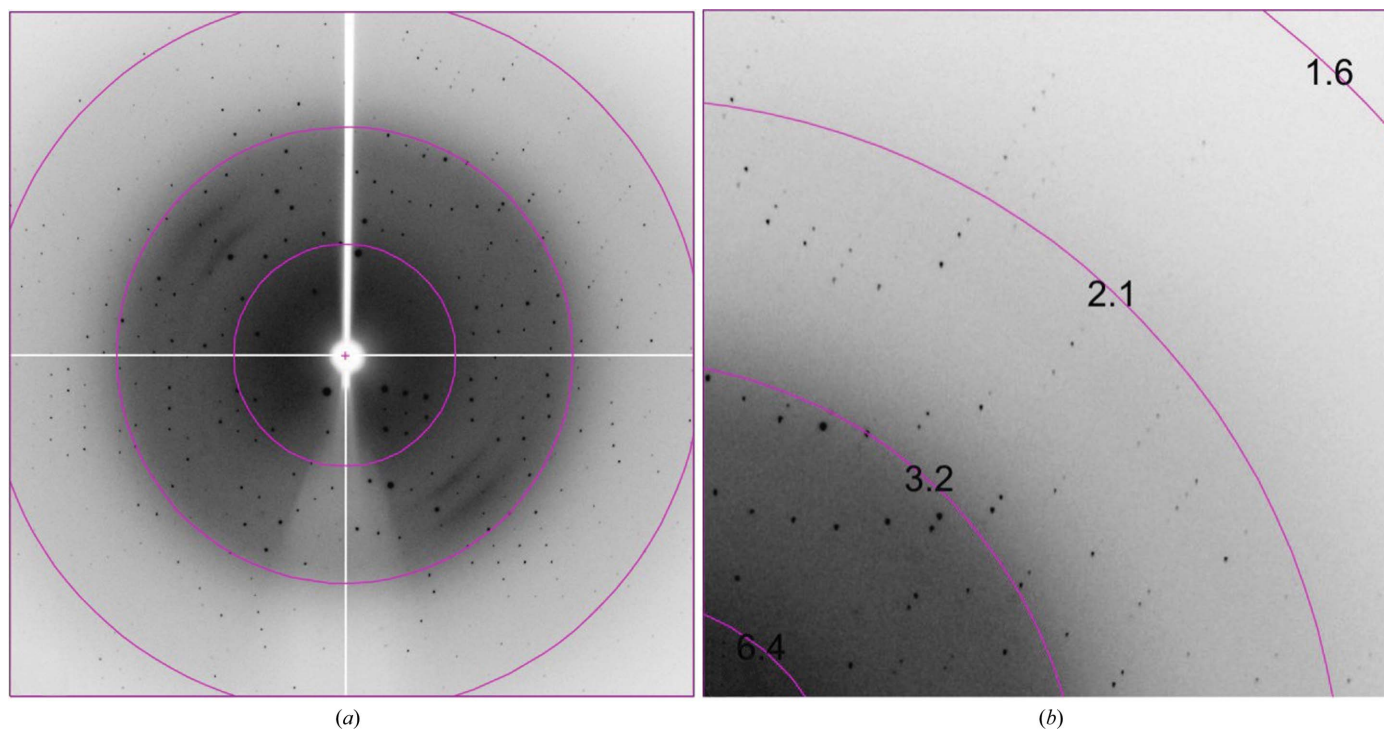
(a)

(b)

Figure 3
Diffraction image of an rIFABP crystal obtained at the Australian Synchrotron.

code 1kzw; Zhang *et al.*, 2003) as a search model. The initial solution had a *Z* score of 5.27 and an initial *R* factor of 0.46, which reduced to 0.35 after ten cycles of restrained refinement using *REFMAC*5. This confirmed the presence of four molecules in the asymmetric unit.

3.2. Rat IFAPB

Crystals of rat IFABP (rIFABP) were obtained from hanging drops using 45%(*w/v*) PEG 2000, 0.1 *M* Tris–HCl pH 7.0, 0.2 *M* MgCl$_2$ at 277 K and grew to dimensions of $0.2 \times 0.15 \times 0.05$ mm (Fig. 1*b*). These crystals were smaller than the hIFABP crystals but were thicker and easier to handle. X-ray diffraction data were collected from an rIFABP crystal to 1.6 Å resolution on beamline MX1 at the Australian Synchrotron (Fig. 3). The crystal-to-detector distance was 150 mm. Data-collection statistics are shown in Table 1. Extra images were collected for this data set to improve the signal-to-noise weak spots observed at the edge of the detector. This led to a multiplicity of 27.7 for this data set and a high $\langle I/\sigma(I) \rangle$ value of 10.1 in the highest resolution bin. After scaling and merging of intensities the crystal was found to belong to space group $P4_32_12$ or $P4_12_12$, with unit-cell parameters $a = b = 50.6$, $c = 97.5$ Å, $\alpha = \beta = \gamma = 90°$. Determination of the structure by molecular replacement with the rIFABP crystal structure (PDB code 2ifb; Sacchettini *et al.*, 1989*a*) confirmed that the crystal belonged to space group $P4_32_12$ with one molecule in the asymmetric unit. The initial solution had a *Z* score of 28.1, with an initial *R* factor of 0.37, which reduced to 0.29 after ten cycles of restrained refinement with *REFMAC*5.

The crystal structures of rIFABP and hIFABP in complex with DAUDA have both been solved and will be reported elsewhere. These results represent a rare situation in which homologous proteins from two different species have been crystallized with the same compound. rIFABP has been used to investigate drug absorption using *in vitro* models of intestinal permeability (Velkov *et al.*, 2007) and rIFABP and hIFABP have been suggested to be suitable for use

in *in vitro–in vivo* extrapolation studies of drug-metabolism kinetics (Rowland *et al.*, 2009). Analysis of the structures will shed light on the the factors that dictate ligand binding and specificity for these two proteins, which will aid in the assessment of their suitability for use in such models.

References

Baier, L. J., Bogardus, C. & Sacchettini, J. C. (1996). *J. Biol. Chem.* **271**, 10892–10896.
Baier, L. J., Sacchettini, J. C., Knowler, W. C., Eads, J., Paolisso, G., Tataranni, P. A., Mochizuki, H., Bennett, P. H., Bogardus, C. & Prochazka, M. (1995). *J. Clin. Invest.* **95**, 1281–1287.
Bernlohr, D. A., Simpson, M. A., Hertzel, A. V. & Banaszak, L. J. (1997). *Annu. Rev. Nutr.* **17**, 277–303.
Chmurzynska, A. (2006). *J. Appl. Genet.* **47**, 39–48.
Collaborative Computational Project, Number 4 (1994). *Acta Cryst.* D**50**, 760–763.
Evans, P. (2006). *Acta Cryst.* D**62**, 72–82.
Furuhashi, M. & Hotamisligil, G. S. (2008). *Nature Rev.* **7**, 489–503.
He, Y., Yang, X., Wang, H., Estephan, R., Francis, F., Kodukula, S., Storch, J. & Stark, R. E. (2007). *Biochemistry*, **46**, 12543–12556.
Leslie, A. G. W. (1992). *Jnt CCP4/ESF–EACBM Newsl. Protein Crystallogr.* **26**.
Lowe, J. B., Sacchettini, J. C., Laposata, M., McQuillan, J. J. & Gordon, J. I. (1987). *J. Biol. Chem.* **262**, 5931–5937.
Marr, E., Tardie, M., Carty, M., Brown Phillips, T., Wang, I.-K., Soeller, W., Qiu, X. & Karam, G. (2006). *Acta Cryst.* F**62**, 1058–1060.

Matthews, B. W. (1968). *J. Mol. Biol.* **33**, 491–497.

McCoy, A. J., Grosse-Kunstleve, R. W., Adams, P. D., Winn, M. D., Storoni, L. C. & Read, R. J. (2007). *J. Appl. Cryst.* **40**, 658–674.

McPherson, A. (1982). *Preparation and Analysis of Protein Crystals.* New York: John Wiley & Sons.

McPhillips, T. M., McPhillips, S. E., Chiu, H.-J., Cohen, A. E., Deacon, A. M., Ellis, P. J., Garman, E., Gonzalez, A., Sauter, N. K., Phizackerley, R. P., Soltis, S. M. & Kuhn, P. (2002). *J. Synchrotron Rad.* **9**, 401–406.

Rowland, A., Knights, K. M., Mackenzie, P. I. & Miners, J. O. (2009). *Drug Metab. Dispos.* **37**, 1395–1403.

Sacchettini, J. C., Gordon, J. I. & Banaszak, L. J. (1989a). *J. Mol. Biol.* **208**, 327–339.

Sacchettini, J. C., Gordon, J. I. & Banaszak, L. J. (1989b). *Proc. Natl Acad. Sci. USA*, **86**, 7736–7740.

Velkov, T., Chuang, S., Wielens, J., Sakellaris, H., Charman, W. N., Porter, C. J. & Scanlon, M. J. (2005). *J. Biol. Chem.* **280**, 17769–17776.

Velkov, T., Horne, J., Laguerre, A., Jones, E., Scanlon, M. J. & Porter, C. J. (2007). *Chem. Biol.* **14**, 453–465.

Young, A. C., Scapin, G., Kromminga, A., Patel, S. B., Veerkamp, J. H. & Sacchettini, J. C. (1994). *Structure*, **2**, 523–534.

Zhang, F., Lucke, C., Baier, L. J., Sacchettini, J. C. & Hamilton, J. A. (2003). *Biochemistry*, **42**, 7339–7347.

Zimmerman, A. W. & Veerkamp, J. H. (2002). *Cell. Mol. Life Sci.* **59**, 1096–1116.